



Article

Mini-Kilns for Charcoal-Making: An Eco-Friendly Solution for Small-Scale Production of Charcoal and Wood Vinegar

Felipe Bento de Albuquerque¹ , Rafael Rodolfo de Melo^{1,*} , Alexandre Santos Pimenta², Edgley Alves de Oliveira Paula¹, Mário Vanoli Scatolino¹ and Fernando Rusch¹

¹ Department of Agronomic and Forestry Sciences, Center for Agrarian Sciences, Federal University of the Semi-arid—UFERSA, Av. Francisco Mota, 572, Costa e Silva, Mossoró 59625-900, RN, Brazil; felipe.albuquerque@alunos.ufersa.edu.br (F.B.d.A.); edgley.paula@alunos.ufersa.edu.br (E.A.d.O.P.); mario.vanoli@ufersa.edu.br (M.V.S.); fe_rusch@yahoo.com.br (F.R.)

² Graduate Program in Forest Sciences, Universidade Federal do Rio Grande do Norte—UFRN, RN 160, Km 03, s/n, Distrito de Jundiaí, Macaíba 59280-000, RN, Brazil; alexandre.pimenta@ufrn.br

* Correspondence: rafael.melo@ufersa.edu.br

Abstract: Charcoal is one of the most essential energy sources in the world and is used mainly for domestic and industrial purposes. Brazilian charcoal production occurs in rudimentary masonry kilns without concern for process safety or energy waste. This work aimed to develop a mini carbonization system of three kilns coupled to a vertical smoke burner for optimized and environmentally correct charcoal and wood vinegar (WV) production on small farms. The project was divided into three parts for dimensioning: the three-kiln set, the WV condensing device, and the smoke burner. The condenser was designed following the procedures from the standards of TEMA (Tubular Exchangers Manufacturers Association); ASME (Society of Mechanical Engineers of the United States) Section VIII, Division 1; and the NR-13 (Regulatory Standard) of ABNT (Brazilian Association of Technical Standards). In contrast to the current scenario, in which primitive carbonization technologies are still employed, bringing about low charcoal yields and significant pollution release, the use of a mini-kiln that allows charcoal production and wood vinegar recovery combined with pollutant smoke burning is an interesting eco-friendly solution. Thus, the mini-kiln model presented here brings a low cost and environmental safety to the charcoal production chain, reaching sustainability parameters and offering higher income opportunities to small producers.

Keywords: charcoal making; carbonization system design; smoke burner; pollution abatement; wood vinegar recovery; socio-environmental impact; sustainable development



Citation: de Albuquerque, F.B.; de Melo, R.R.; Pimenta, A.S.; de Oliveira Paula, E.A.; Scatolino, M.V.; Rusch, F. Mini-Kilns for Charcoal-Making: An Eco-Friendly Solution for Small-Scale Production of Charcoal and Wood Vinegar. *Inventions* **2023**, *8*, 146. <https://doi.org/10.3390/inventions8060146>

Academic Editors: Umberto Lucia, Giulia Grisolia and Debora Fino

Received: 9 October 2023

Revised: 11 November 2023

Accepted: 13 November 2023

Published: 17 November 2023



Copyright: © 2023 by the authors. Licensee MDPI, Basel, Switzerland. This article is an open access article distributed under the terms and conditions of the Creative Commons Attribution (CC BY) license (<https://creativecommons.org/licenses/by/4.0/>).

1. Introduction

Charcoal is among the most relevant energy sources worldwide, and it is directed to several purposes, including household, medicinal, and industrial end uses [1]. Besides providing energy as heat for domestic uses, it can act as a reductant of iron ore in metallurgical blast furnaces with efficiency and sustainability [2]. In Brazil, 40% of steel, 70% of pig iron, 100% of iron alloys, and 100% of metallic silicon are produced with charcoal as a carbon source [3], while in every other country, they are manufactured using coke. Even though metallic commodities are made using cutting-edge technologies, the charcoal that feeds the industries in this sector is produced mainly in rudimentary and low-tech masonry kilns [4]. In those kilns, the losses of bone-dry firewood in mass and energy correspond to 65 and 50%, respectively. Wood carbonization dates back thousands of years. Also called slow pyrolysis, this process consists of thermal decomposition in which wood is subjected to a heating rate under a low-content or oxygen-free atmosphere, so the raw material does not burn but only decomposes by the action of the heat, in times ranging from hours to days [5,6]. Through the carbonization of wood, agricultural waste products of other lignocellulosic materials are processed, yielding three types of products, as follows: solids

(charcoal itself), liquids (wood vinegar and tar), and gases (CO , CO_2 , H_2 , and CH_4) [7–9]. In the day-to-day carbonization process carried out with low-tech kilns, charcoal is usually the only product of interest and the other products are released as smoke into the surrounding atmosphere, constituting, in most cases, a severe source of pollution. Still, the yield in pyrolysis coproducts depends on wood type and operational conditions such as heating rate, final temperature, the raw material's moisture content, and labor skills [1]. Therefore, the control of the process is entirely subjective, relying on personal perceptions about the external temperature of the kiln and the smoke color, which changes as the carbonization goes on. The control of the process also depends on the type of kiln [10].

One of the prevalent strategies is to add value, to promote the circular economy and provide a suitable harnessing of the carbonization coproducts. In agriculture, WV can be used as an insecticide, fungicide, bactericidal, crop growth promoter, and so on [11–14]. Also, using WV as a preservative, a source of chemicals, and a basis for veterinary products has been accomplished [15–17]. Another carbonization coproduct, wood tar, has been studied as biofuel [18–20]. As pointed out above, releasing carbonized smoke as pollution demands some device to decrease it, so the kilns reach environmental compliance. Smoke burners are the most suitable devices, which can thermally destroy the chemicals from the smoke, turning them into carbon dioxide and water. Bearing these points in mind, coupling WV and wood tar recovery apparatus and smoke burners to carbonization kilns is desirable, from an environmentally friendly standpoint. It adds value to the charcoal production chain. When the smoke is burned after WV recovery, the release of CH_4 is eliminated, which is an advantage since this component strongly contributes to greenhouse gas emissions. Methane can cause 21 times more greenhouse effects than carbon dioxide [21]. This is essential to consider if the interest is to obtain carbon credits from the carbonization process.

Considering better efficiency of the charcoal-making process, pollution reduction, and coproduct recovery should be considered complementary and necessary to make the global process more economically rational and eco-friendly. Several studies have been conducted to design smoke burners and devices to recover carbonization liquids to reach these goals [22–25]. A total game changer is emerging from these new approaches to mitigate the adverse effects of charcoal-making and optimize its energy and mass global yields. In Brazil and even worldwide, more than 80% of charcoal is produced by small and medium farmers, and due to their restricted investment capacity and access to technologies, they usually choose low-tech kilns to meet their productive needs. Those kilns are cheap and do not demand a highly skilled labor force but have a low volumetric capacity and release significant amounts of pollutant smoke. Besides, firewood loading and charcoal unloading are entirely manual, demanding a considerable physical effort by workers. To make things worse, the rudimentary kilns are built based on local traditions, following models without design or calculations.

In this context, this work aimed to propose an innovative carbonization system (CS), consisting of three masonry kilns coupled to a central WV recovery system connected to a vertical smoke burner. This carbonization system was designed to be environmentally clean and to provide WV and charcoal in the same production line. Small and medium charcoal makers and rural farmers can be directed to use the carbonization system proposed here.

2. Materials and Methods

The design steps of the CS are described as follows. Each component of the carbonization system was addressed separately for a better understanding of the reader, and the design was thoroughly depicted step by step, including calculations and project drawings. The CS components are kilns, a WV recovery device, and a smoke burner. To conclude, the complete design containing all the components connected was presented.

2.1. Project Premises

The average pyrolysis time is roughly eight days. It takes three days for carbonization and five days for charcoal cooling to occur. During the rainy season, the carbonization

process can usually take four days to be concluded. However, the total process time does not change because the rain decreases the time needed for charcoal cooling. So, the time distribution for each process step is as follows:

- ✓ Firewood loading: 2 h;
- ✓ Carbonization time: 72 h (3 days);
- ✓ Charcoal cooling: 120 h (5 days);
- ✓ Charcoal unloading: 2 h;
- ✓ Total: 196 h.

The steps above are displayed in Figure 1. Taking advantage of the process cycle, a set of three kilns was designed, to optimize charcoal-making and maintain its production without interruption, as well as the WV recovery. This way, there is always one kiln carbonizing, one kiln with charcoal cooling, and another undergoing charcoal unloading and firewood loading. Once one charring run ends, another occurs, and the process continues.

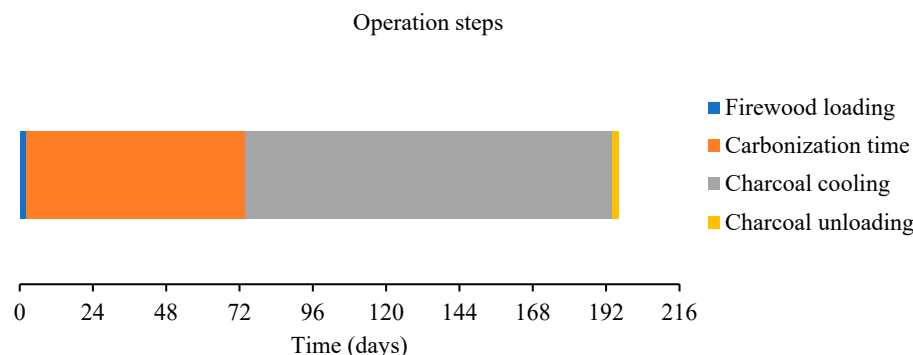


Figure 1. Stages of mini-kiln operation.

The cycle is summarized as follows. Kiln one starts to run, and three days later, charcoal-making and WV recovery are interrupted, and charcoal cooling starts (3 + 5 days cycle). At this point, kiln two immediately starts to work, and in turn, the carbonization process finishes three days later. Like kiln one, the charcoal cooling will take five days (3 + 5 days cycle). Finally, kiln three goes into work with the same process characteristics (3 + 5 days cycle). On the 8th day, the production cycle restarts for each kiln; therefore, the 3-kiln set works continuously (Figure 2).

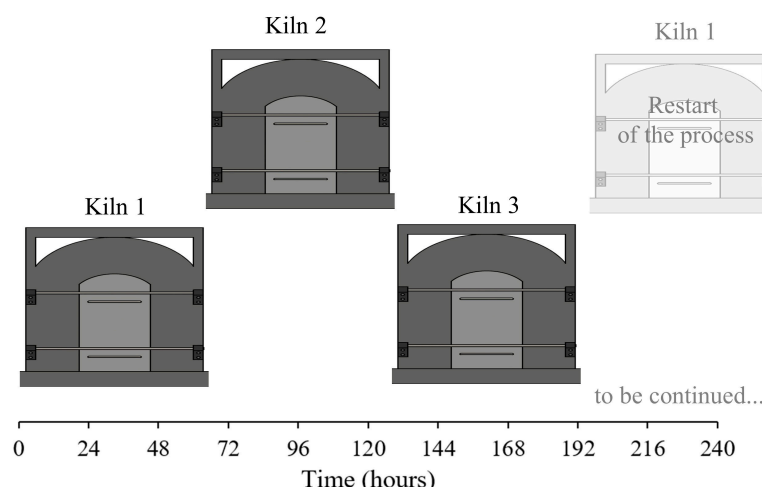


Figure 2. Charcoal and wood vinegar production in the mini-kiln over time.

As commented above, each part and its respective design and dimensioning are presented in the following items.

2.2. Carbonization Kilns

The carbonization kilns were built with solid red ceramic bricks (180 mm length × 90 mm width × 57 mm thickness) laid using mortar composed of clay soil, sand, and water, according to the standard NBR 15270-1 [26]. The kiln dimensions were 3130 mm in length × 1790 mm in width × 2310 in height. They were placed on a reinforced concrete (30 MPa) base measuring 14,500 mm in size × 5380 mm in width × 260 mm in thickness. Around the upper part of the kiln walls was a concrete beam completely enfolding the structure to hold up the dome. The dome was 500 mm in height, had built-in red ceramic bricks, and was covered with a 50 mm reinforced concrete slab directly connected to the steel reinforcement of the beam. Each kiln had five holes, four of them located at the basis of opposite lateral walls and one at the top of one of these walls. This last hole ignited the firewood load, and the two others controlled the air intake during the carbonization process.

Each kiln was connected to the WV recovery system through an aerial masonry duct with the external measures of 550 mm in width × 400 mm in height. The smoke duct was built with the same type of brick and mortar employed in the kiln walls and dome. An internal free space (150 mm in diameter) allowed the pyrolysis gases to be driven to the WV condensing system. Each kiln had a door made of reinforced concrete (30 MPa) measuring 1500 mm in height × 550 mm in width × 50 mm in thickness. After the firewood was loaded, the door was closed and sealed with plastic clay, and the kiln was ready to be ignited so the carbonization process could start.

2.3. Condensing System for WV Recovery

The sizing of the condensing system initially consisted of preparing an analytical project, which included defining the type of fluid, pressure, temperature, flow rate, specific heat of water, and enthalpy in both operating and design conditions. For the thermal design, the definition of the type of equipment, the heat exchange areas, the quantity, arrangement, and spacing of internal tubes, and the mechanical design were considered when selecting materials for hull and lids construction. To prepare the mechanical and thermal project, the following standards were used as a basis: American Association of Heat Exchanger Manufacturers [27], Society of Mechanical Engineers of the United States [28], and NR-13—Boilers, Pressure Vessels, Pipes, and Metallic Storage Tanks [29]. These standards establish requirements and recommendations for the design, material selection, testing, installation, safety, and operation of heat exchangers and pressure vessels. Also, the analyses described by Telles [30] and Cengel and Cimbala [31] were adopted for the mechanical and thermal projects, respectively.

In addition to all accessory parts such as flanges, nozzles, supports, mirrors, screws, and other internal and external elements, the need or not for corrosion margins (extra thickness), the final dimensions of the device, and the structural calculation including the thickness of all pressure parts were considered, as well as reinforcements, the maximum allowable working pressure (PMTA) and the hydrostatic test pressure (TH), so the complete mechanical drawing of the system could be carried out. In the context presented above, a water-cooled heat exchanger was proposed. The condenser is a multitube type, allowing the pyrolysis gases to pass only once through each one. It is widely used in industry, easy to assemble, and permits multiple configurations, applied to various types of services and in different pressure and temperature ranges. The condenser was vertically positioned and had its basic structure consisting of a cylindrical hull involving a set of tubes. This arrangement was chosen due to the ease of manufacturing, transport, and economy. Considering economic factors, two fixed flat tops and supports for columns were chosen. The condensing section comprised a bundle of parallel steel tubes strategically distributed inside the hull so the pyrolysis gases could freely pass through them, leaving behind their condensable fraction. This way, the carbonization smoke is admitted at the bottom of the condenser and exits at the top part. The tubes are water-cooled, and the fluid is always kept at 25–30 °C. The carbonization gases flow in a countercurrent mode throughout the

tubes, leaving the liquid products behind as the smoke moves up. The tubes were built straight so the smoke could pass freely, preventing the occurrence of any clogging by wood tar deposition.

2.3.1. Condensing System Design

In this step, the sizing of the condensing system was carried out, and factors like manufacturing and maintenance easiness, installation, work safety, economics, and the past experiences of other researchers [32–34] were considered. To obtain the pressure hull ($P_{op_hull_int}$), the reservoir was considered to be full of water from the upper to its top parts at the height of the cooling water outlet. At this point, the highest influence of the liquid column was defined by the sum of the gauge pressure (P_{man}), referring to the water column and the atmospheric pressure (P_{atm}) [23]. According to Equation (1), we have:

$$P_{op_hull_int} = P_{man} + P_{atm} \quad (1)$$

Knowing Equation (2):

$$P_{man} = \rho \cdot g \cdot h \quad (2)$$

where ρ is the specific mass of water (kg m^{-3}), g is the acceleration of gravity (m s^{-2}), and h is the manometric height or head (m).

For the specific mass of water, the value of 1000 kg m^{-3} was considered, and for the acceleration of gravity, 9.81 m s^{-2} with a head of 0.8 m was considered. Substituting the values into Equation (2), we have:

$$P_{man} = 1000 \text{ kgm}^{-3} \cdot 9.81 \text{ ms}^{-2} \cdot 0.8 \text{ m}$$

Therefore,

$$P_{man} = 7.85 \text{ kPa}$$

With that established, knowing that P_{atm} equals 101.32 kPa (1.03 kgf/cm^2 or 1 atm) in the upper part of the liquid column, and substituting the values into Equation (1), we have:

$$P_{op_hull_int} = 7.85 \text{ kPa} + 101.32 \text{ kPa}$$

$$P_{op_hull_int} = 109.17 \text{ kPa} \text{ or } (1.11 \text{ kgf cm}^{-2})$$

The operating pressure on the outside of the hull was atmospheric pressure (P_{atm}). The working pressure inside the tubes ($P_{op_int_tubes}$) was also considered atmospheric pressure, since this system is connected directly to the burner, which is open to the atmosphere. Still, the design pressure for the hull (P_{p_hull}) was defined as recommended by ASME [28], whereas, in the case of vessels designed for internal pressure, the design pressure (P_{p_int}) was adopted as the highest of the two values according to the following conditions: maximum operating pressure, increased by 5% when the pressure relief device (safety valve) is operated by a pilot valve and increased by 10% in other cases; 147.10 kPa of head. The second condition was chosen in the analyzed situation because it is more critical and increases the safety factor. It was necessary to add the atmospheric press value (P_{atm}), according to Equation (3):

$$P_{p_hull} = P_{p_int} + P_{atm} \quad (3)$$

Substituting the values of P_{p_int} and P_{atm} into Equation (3), we have:

$$P_{p_hull} = 147.10 \text{ kPa} + 101.32 \text{ kPa}$$

$$P_{p_hull} = 248.42 \text{ kPa} \text{ or } 2.53 \text{ kgf cm}^{-2}$$

As the hull design pressure (P_{p_hull}) was defined for the internal part, it was observed that this same pressure acts on the external part of the tube set itself. Furthermore, it was

higher than the interior design pressure of the pipes ($P_{p_int_tubes}$), which was 147.10 kPa (1.5 kgf cm⁻²), according to ASME [28], also defined as the design pressure for the tubes (P_{p_tubes}). The operating temperature at the entrance to the hull ($T_{op_ent_hull}$) was the inlet temperature of the water at ambient temperature (25 °C). In comparison, the operating temperature at the hull exit ($T_{op_exit_hull}$) assumed the value of 45 °C, so the heat exchanger could operate with a slight temperature difference. We avoided designing a compensation system for expansion in the equipment, which would generate additional costs [30]. The values for the operating temperatures at the inlet and outlet of the tubes ($T_{op_ent_tubes}$) and ($T_{op_out_tubes}$) had equal values because the system is a condenser where heat is exchanged. Therefore, the condensation of pyrolysis liquids occurs at a constant temperature, considering the maximum value of 115 °C as the average temperature to recover the WV [35].

The system provided a water flow rate of 1.5 kg s⁻¹ (1.5 L s⁻¹). The average specific water heat at 35 °C was 4.178 (kJ kg⁻¹ K⁻¹), according to [31]. The mass flow rate of the gases was estimated at 0.0025 kg s⁻¹. The specific heat of pyrolysis gases was not defined precisely since it comprises various chemical components [36]. According to Pires et al. [37], there may be more than 300 chemical components in the composition of carbonization gases. This diversity makes it challenging to define the characteristic patterns of these gases [36,38,39]. With all that said, the operating and design features of the condensing system are shown in Table 1.

Table 1. Operational features of the condensing system of WV.

Fluid	Hull	Tubes
	Water	Carbonization Gases
Internal operating pressure (P_{op_int})	109.17 kPa	101.32 kPa
External operating pressure (P_{op_ext})	101.32 kPa	109.11 kPa
Design pressure (P_p)	248.42 kPa	248.42 kPa
Inlet operating temperature (T_{op_inlet})	25 °C	115 °C
Outlet operating temperature (T_{op_out})	45 °C	115 °C
Design temperature (T_p)	65 °C	150 °C
Mass flow (m)	1.5 kg s ⁻¹	0.0025 kg s ⁻¹
Specific heat (c_p)	4.178 kJ kg ⁻¹ K ⁻¹	-

2.3.2. Thermal Design of the Condensing System

The thermal design of the condensing system, a heat exchanger, basically consisted of determining the internal tube set's heat exchange area, quantity, arrangement, and spacing. To size the system, the following considerations were made, following the recommendations of Cengel and Cimbala [31]: (a) heat exchangers are considered as steady flow equipment, since they usually operate for long periods without any changes in their operating conditions (mass flow, temperature, and flow speed); (b) fluid flows have little or no change in their speeds, so changes in kinetic and potential energy are insignificant; (c) heat conduction in the axial direction is insignificant and therefore negligible; (d) the external surface of the heat exchanger is considered perfectly insulated, with no heat exchange with the environment; and (e) heat exchange occurs only between the two fluids. To determine the heat exchange area and number of tubes, the logarithmic mean temperature difference method (LMTD), as seen in Equation (4), was employed:

$$\dot{Q} = U \cdot A_s \cdot \Delta T_{ML} \quad (4)$$

where \dot{Q} is the global heat transfer rate (W), U is the global heat transfer coefficient (W m⁻² K), A_s is the heat transfer area (m²), and ΔT_{ML} is the logarithmic temperature mean difference (K).

The first law of thermodynamics was used to calculate the heat transfer rate. As such, the heat transfer rate from the hot fluid must equal the heat transfer rate to the cold liquid; thus, Equation (5) can be employed for water:

$$\dot{Q} = \dot{m}_f \cdot c_{pf} \cdot (T_{f,sai} - T_{f,ent}) \quad (5)$$

where \dot{m}_f is the mass flow rate of the cold fluid (kg s^{-1}), c_{pf} is the specific heat of the cold fluid ($\text{kJ kg}^{-1} \text{K}^{-1}$), $T_{f,sai}$ is the cold fluid exit temperature (K), and $T_{f,ent}$ is the cold fluid inlet temperature (K).

Because a part of the carbonization gases is undergoing a phase change process and turning into liquids, calculating the heat transfer rate can also be undertaken using Equation (6):

$$\dot{Q} = \dot{m}_q \cdot h_{fg} \quad (6)$$

where \dot{m}_q is the mass flow rate of the hot fluid (kg s^{-1}) and h_{fg} is the enthalpy of vaporization (kJ kg^{-1}).

Based on previous carbonization runs, the mass flow rate of the gases was the estimated value referring to processing roughly 650 kg of wood in 72 h, equivalent to a value of 0.0025 kg s^{-1} . Due to the composition of the carbonization gases, which makes it difficult to determine the enthalpy of vaporization at the specified temperature, Equation (5) was used to calculate the heat transfer rate. In Equation (5), a value of $4.178 \text{ kJ kg}^{-1} \text{ K}^{-1}$ was used, corresponding to the specific heat value for water at 35°C (the mean temperature between 45 and 25°C) [31]. The cold fluid's mass flow rate was considered, corresponding to a commercial centrifugal pump with an average flow value of 1.5 L s^{-1} with a power of 0.5 CV , a head of 3 m , suction, and a discharge diameter of 0.75 inches [40]. In addition, the values of 25°C (298.15 K) and 45°C (318.15 K) were also considered for the water inlet and outlet temperatures, respectively. These values are based on heat exchangers, like those cited by [31]. Substituting the values into Equation (5), we have:

$$\dot{Q} = 1.5 \cdot 4.178 \cdot 20$$

$$\dot{Q} = 125.34 \text{ kW}$$

To determine the global heat transfer coefficient, an approximation of the reference values proposed by Cengel and Cimbala [31] was carried out, due to the difficulty in determining the value of the convection heat transfer coefficient for carbonization gases and the fouling factor. The estimated value was $1000 \text{ W m}^{-2} \text{ K}^{-1}$, referring to the steam condenser, as it is close to the objective of the equipment, which is the condensation of wood vinegar. To calculate the logarithmic mean temperature difference, Equation (7) was used, considering a countercurrent flow:

$$\Delta T_{ML} = \frac{\Delta T_1 - \Delta T_2}{\ln(\Delta T_1 / \Delta T_2)} \quad (7)$$

where ΔT_1 and ΔT_2 represent the temperature differences between the two fluids at both ends (inlet and outlet) of the heat exchanger. For a countercurrent flow, they are defined by Equations (8) and (9) below:

$$\Delta T_1 = T_{q,ent} - T_{f,sai} \quad (8)$$

$$\Delta T_2 = T_{q,sai} - T_{f,ent} \quad (9)$$

where $T_{q,out}$ is the hot fluid outlet temperature (K) and $T_{q,inlet}$ is the hot fluid inlet temperature (K). Substituting the values into Equations (8) and (9), we have:

$$\Delta T_1 = 115 - 45 = 70^\circ\text{C}$$

$$\Delta T_2 = 115 - 25 = 90 \text{ } ^\circ\text{C}$$

Finally, the values of ΔT_1 and ΔT_2 can be applied in Equation (7). Therefore, we have:

$$\Delta T_{ML} = \frac{70 - 90}{\ln(70/90)} = 80 \text{ } ^\circ\text{C}$$

To determine the surface area of the heat exchanger, we substituted the values of the \dot{Q} , U , and ΔT_{ML} into Equation (4):

$$125,340 \text{ W} = 1000 \text{ W/m}^2 \cdot K \cdot A_s \cdot 80 \text{ } ^\circ\text{C}$$

$$A_s = 1.56675 \text{ m}^2$$

Considering factors such as weight, a better distribution of the heat exchange area, ease of manufacturing, and cost, the heat exchanger's surface area was distributed in 25 tubes, measuring 0.8 m in length each. The heat exchange surface area of each tube ($A_{p/tube}$) was determined using Equation (10):

$$A_{p/tube} = \frac{A_s}{N} \quad (10)$$

where N is the number of tubes. Substituting the values into Equation (10), we have:

$$A_{p/tube} = \frac{1.56675}{25} = 0.06267 \text{ m}^2$$

Then, to determine the diameter of each tube ($D_{p/tube}$), Equation (11) was used:

$$A_{p/tube} = \pi \cdot D_{p/tube} \cdot L \quad (11)$$

Substituting the value of $A_{p/tube}$ we have:

$$D_{p/tube} = \frac{0.06267}{\pi \cdot 0.8} = 0.02495 \text{ m or } 24.95 \text{ mm}$$

Approaching the value of the largest and closest nominal diameter (DN), the value of 1 inch (25.4 mm) was found. Therefore, they were manufactured from ASTM A-179 [41] carbon steel, following the recommendation of [28]. According to TEMA [27], the spacing between the centers of neighboring tubes must be at least 1.5 times the external diameter of the tubes. A minimum of 6 mm free distance between tubes is required for square or quincunx arrangements. Therefore, considering that the value of the external diameter of the heat exchanger tubes calculated by Equation (11) was 25.4 mm, the spacing between tube centers will be 1.5×25.4 , namely 38.1 mm, determining the free distance between the tubes to be 12.7 mm. Thus, it is more sensible to adopt the arrangement of the heat exchanger tubes in a squared configuration. With the definition of the layout of the heat exchanger tube arrangement, the internal diameter of the hull ($d_{int,hull}$) was placed in the Pythagorean theorem to determine the distance (A), dividing the square formed into two right triangles to allow for the calculation of the longest edge (hypotenuse). Knowing that the spacing between tube centers is 38.1 mm, the values of edges B and C are equal to 4×38.1 , namely 152.4 mm; therefore, substituting the values in the Pythagorean theorem equation, we have:

$$A = \sqrt{152.4^2 + 152.4^2} = 215.53 \text{ mm}$$

Furthermore, as the calculated value was found to be equivalent to center-to-center of the tubes, it was necessary to add 25.4 mm to this value, corresponding to twice the radius (12.7 mm), to determine the highest distance (end of the tube in the bottom left to

the end of the other tube in the top right—see Figure 2), which totals 240.93 mm. With the value of the internal diameter calculated [27,30], the minimum wall thickness of the tube is required to be “Series 30” (designation of tube wall thickness recommended by the ASME B31.3 [42]). The minimum internal diameter and wall thickness values can be determined using the most significant and closest commercial values. Telles [43] and Telles [30] established nominal values for dimensions and weights of carbon steel tubes for use in industry. Thus, they pointed out that the calculated internal diameter is within the range of commercial inner diameters for the nominal diameter of 10 in, which corresponds to 273 mm. Considering the minimum wall thickness (Series 30) required by TEMA [27], the previous commercial internal diameter (d_i) of 254.5 mm is established, with a prior wall thickness of 9.27 mm corresponding to “Series 40” or “Std”. These previous values will be confirmed or not with the calculation of the minimum hull wall thickness determined by the mechanical design.

2.3.3. Mechanical Design of the Condensing System

To prepare the mechanical design of the condenser (heat exchanger), the TEMA [27] was used, complementing the conditions described by [28]. Therefore, the final design met all the requirements stated by these references. The condensing system was classified as class C, referring to equipment subjected to services of moderate risk and responsibility, considering economic conditions. The type of steel used to manufacture the hull was ASTM A53 Gr A [44], due to its degree of operational responsibility, availability, cost, and researchers' experiences of it in previous projects. Furthermore, the non-detachable tube bundle was adopted, being arranged rectally, due to the nature of the gases, which are prone to generating incrustations and consequently clogging, in addition to facilitating cleaning [30]. The mirrors were fixed, a condition that allowed the system to function without the provisions for compensating for differential thermal expansion. Since the system was composed of different components (top and bottom caps, hull, mirrors, and tubes set), the specifications of allowable tensions were adopted, all of them made in carbon steel and a working temperature of 150 °C, following the recommendations of the ASME [28]. So, the materials adopted to build each part of the condensing system were as follows: (a) caps: carbon steel A-285 Gr C, with an allowable stress of 108 MPa; (b) hull: A-53 Gr A, with an allowable stress of 80.6 MPa; (c) mirrors: A-285 Gr C, with an allowable stress of 108 MPa; and (d) tubes set: A-179, with an allowable stress of 92.3 MPa. The allowable tension values for all parts did not vary with temperature changes (ambient up to 150 °C), as stated by [28].

Hull Sizing

According to ASME [28], to calculate the wall thickness of the condensing system hull, considering the internal pressure, Equations (12) and (13) presented below were used, and we selected the one with the highest value. In the present case, when it comes to top welding performed on both sides of the steel plate edges or equivalent procedure, a value equal to one was considered to be the E parameter (Equation (12)) to obtain total fusion and penetration without limitations and with a degree of inspection able to be inspected by radiography. For the parts subjected to pressure (hull, tube set, and mirrors), a corrosion margin (over-thickness) of 3 mm was included, as the working medium (water and gases) was considered corrosive to a medium degree, especially when considering the little or no maintenance that the vase will receive throughout its lifespan.

$$T_{\text{hull1}} = \frac{P \cdot R}{S_{\text{hull}} \cdot E - 0.6 \cdot P} + C_{\text{hull}} \quad (12)$$

$$T_{\text{hull2}} = 2.5 + 0.001D_i + C_{\text{hull}} \quad (13)$$

where T_{hull} is the minimum thickness needed to resist internal pressure (m), P is the design internal pressure, adding the effect of the head when necessary (Pa), R is the inner

radius of the cylinder (m), S is the allowable stress of the material (Pa), E is the welding efficiency coefficient, C is the corrosion over-thickness (m), and D_i is the inner diameter of the hull (mm).

The value of the internal design pressure (P), according to Table 1, was 248.42 kPa, the inner radius (R) was 127.25 mm, and the allowable stress of the material (S) was 80.6 MPa. Substituting these values into Equation (12), we have:

$$T_{\text{hull}1} = \frac{248.42 \cdot 10^3 \cdot 0.12725}{80.6 \cdot 10^6 \cdot 1 - (0.6 \cdot 248.42 \cdot 10^3)} + 0.003 = 3.39 \cdot 10^{-3} \text{ m or } 3.39 \text{ mm}$$

Substituting the values into Equation (13), the result is:

$$T_{\text{hull}2} = 2.5 + (0.001 \cdot 254.5) + 3 = 5.75 \text{ mm}$$

Considering the standard [27] requirements, the minimum thickness values must be "Series 30", regardless of the calculated values. Therefore, the values of the nominal diameter (10 in), internal diameter (254.5 mm), and wall thickness (9.27 mm corresponding to "series 40" or "Std"), previously determined in Section 2.3.2, meet the specification.

Tube Set Sizing

Two calculations were carried out to determine the wall thickness of the tube set and follow the ASME [28] recommendations. One was for external pressure and the other was for internal pressure. Considering the tube set as if it were a cylindrical hull and, therefore, using Equations (12) and (13), the one with the highest value was selected. Checking Table 1, the internal design pressure (P) for both internal and external sides equaled 248.42 kPa. So, for internal pressure, considering that R equals 0.0127 m, S equals 92.3 MPa (Table 1), and E equals one, and knowing that, for ASME [28], it is not necessary to add any corrosion allowance for the tube set ($C = 0$), by substituting the values into Equation (12), we have:

$$T_{\text{tube_set_p_int}1} = \frac{248.42 \cdot 10^3 \cdot 0.0127}{92.3 \cdot 10^6 \cdot 1 - (0.6 \cdot 248.42 \cdot 10^3)} + 0 = 3.42 \cdot 10^{-5} \text{ m or } 0.0342 \text{ mm}$$

Calculating the same parameter using Equation (13), the result is:

$$T = 2.5 + (0.001 \cdot 25.4) + 0 = 2.52 \text{ mm}$$

The calculation of the wall thickness of the tube set, considering the external pressure, according to ASME [28], was developed through successive approximations. Initially, a value for wall thickness was determined, and then the relationship between the external diameter (D_0) and the wall thickness (e) was calculated using Equation (14):

$$\frac{D_0}{T} \quad (14)$$

Considering that the D_0 is 25.4 mm (according to Section 2.3.2) and arbitrating the value of 0.3 mm for wall thickness (e), the value of the relationship was 84.67 mm, a value that is compatible in the sizing stage for cylinders with a D_0/e ratio ≥ 10 . Next, the value of the ratio of the length of the tubular set (L) and the external diameter (D_0) was determined using Equation (15):

$$\frac{L}{D_0} \quad (15)$$

As L is 800 mm (according to Section 2.3.2), a ratio value equal to 31.5 was found. This value was used to determine FACTOR A and then FACTOR B, to determine the maximum allowable working pressure (external MAWP) for the tube set in MPa, according to recommendations by TEMA [27] and Telles [30]. The value of FACTOR A found was

approximately 0.0002. The value of FACTOR B found was roughly 18. Then, the MAWP was calculated using Equation (16):

$$\text{MAWP}_{\text{external}} = \frac{4 \cdot B}{3(D_0/T)} \quad (16)$$

Substituting the values, we have:

$$\text{MAWP}_{\text{external}} = \frac{4 \cdot 18}{3(2.4/0.3)} = 0.283 \text{ MPa}$$

Finally, as the maximum allowable external pressure is slightly higher than the vessel's design external pressure (0.248 MPa), the arbitrated value for thickness ($T = 0.3 \text{ mm}$) met the recommendations from the ASME [20] standard. Thus, considering the tube thickness values calculated for internal ($T = 2.52 \text{ mm}$) and external ($T = 0.3 \text{ mm}$) pressure, the highest value was chosen when subjected to internal pressure. Thus, considering the commercial wall thickness higher and closer to the calculated value [27,30], the selected value for the tube set (heat exchanger part) was 2.77 mm.

Maximum Allowable Working Pressure (MAWP)

Two calculations were necessary to determine the MAWP of the condensing system; one for the external portion of the tube set (defined by Equation (16) previously) and another for the hull's interior. Therefore, to determine the MAWP inside the hull ($\text{MAWP}_{\text{hull}}$), Equation (17) was used, according to ASME [28]:

$$\text{MAWP}_{\text{hull}} = \frac{S_{\text{hull}} \cdot E \cdot T}{R + 0.6 \cdot T} \quad (17)$$

where the wall thickness (T) is the highest calculated value of T_{hull1} and T_{hull2} , and the values of T and S correspond to the design condition. Considering that the allowable stress of the hull material (S) at room temperature was equal to 80.6 MPa, the welding efficiency coefficient (E) was equal to 1, hull wall thickness (e) was equal to 0.00575 m (calculated), and the internal radius of the hull (R) was equal to 0.12725 m, when we substitute these values into Equation (17), we have:

$$\text{MAWP}_{\text{hull}} = \frac{S \cdot E \cdot T}{R + 0.6 \cdot T} = \frac{80.6 \cdot 10^6 \cdot 1 \cdot 0.00575}{0.12725 + (0.6 \cdot 0.00575)} = 3,545,906.66 \text{ Pa or } 3.54 \text{ MPa}$$

Therefore, at the end of the calculations to determine the MAWP of the condensing system, it was observed that the lowest value is the external MAWP (0.283 MPa), which was, therefore, the determined value of the equipment for this parameter.

Mirrors Sizing

The thickness of the heat exchanger mirror plate must be calculated separately [27] for the pressure acting on each side (pressure in the hull and pressure in the tubes), which are working in isolation. The mirror plate's nominal thickness (T_m) must be, at least, the highest of the two calculated values. In the heat exchanger under analysis, the design pressure is the same for both the shell and the tube bundle ($248.42 \times 103 \text{ Pa}$), as per Table 1, making it necessary to carry out the calculation to determine the mirror thickness only once. From Equations (18) and (19) below, the value of T is selected:

$$T_{m1} = T + C_c + C_t \quad (18)$$

$$T_{m2} = T + C_c + R_c \quad (19)$$

where T_m is the effective thickness calculated for the mirror (m), C_c is the corrosion over-thickness on the hull side (m), C_t is the corrosion over-thickness of the tubes (m), and R_c is the depth of the slot for fitting the baffles (m).

The value of T was calculated from Equations (20) and (21) below, considering the effects of bending and shear, respectively, and the higher of the two calculated values was adopted.

$$T = \frac{F \cdot G}{3} \cdot \sqrt{\frac{P}{n \cdot S}} \quad (20)$$

$$T = \frac{1.24 \cdot A}{C \cdot \left(1 - \frac{d_0}{b}\right)} \cdot \left(\frac{P}{S}\right) \quad (21)$$

where T is the effective thickness of the mirror (m), P is the design pressure (Pa) on the hull or tube side, S is the allowable stress of the material (Pa), C is the perimeter formed by the line passing through the centers of the outermost tubes of the mirror, A is the area included within the perimeter C (m^2), F and G are numerical coefficients used for mirrors that have sealing joints on both sides: firstly, fixed and floating mirrors, for straight tubes, where F is one and G is the average diameter of the mirror sealing joint (m); and, secondly, fixed mirrors for U-shaped tubes, where F is 1.25 and G is the average diameter of the mirror sealing joint (m). Additionally, n is the values indicated, according to Equation (22) for square arrangements [27]:

$$n = 1 - \left[\frac{0.785}{\left(\frac{b}{d_0}\right)^2} \right] \quad (22)$$

where b is the distance from center-to-center of the tubes (m) and d_0 is the external diameter of the tube set (m).

Since the value of b was 0.0381 m (as shown in Figure 1) and d_0 was 0.0254 m (as determined in Section 2.3.2), substituting these values into Equation (22) leads to:

$$n = 1 - \left[\frac{0.785}{\left(\frac{0.0381}{0.0254}\right)^2} \right] = 0.6511$$

Then, the T value for bending and shear was calculated using Equations (20) and (21), respectively. For bending, considering that for the fixed mirror ($F = 1$), G is 0.2545 m, P is 248.42 kPa (Table 1), and S is 108 MPa, we have:

$$T_m = \frac{1 \cdot 0.2545}{3} \cdot \sqrt{\frac{248.42 \cdot 10^3}{0.6511 \cdot 108 \cdot 10^6}} = 0.005042 \text{ m or } 5.042 \text{ mm}$$

For shear, the value of A was determined by calculating the area of the square formed by the arrangement of the tube set as shown in Figure 1; each side of the square has a length equal to 0.1524 m, thus, A is 0, and $1524 \text{ m} \times 1524 \text{ m}$ is 0.023225 m^2 . The value of C was 0.1524×4 , namely 0.6096 m. Therefore, substituting the values into Equation (21), we have:

$$T_m = \frac{1.24 \cdot 0.023225}{0.6096 \cdot \left(1 - \frac{0.0254}{0.0381}\right)} \cdot \left(\frac{248.42 \times 10^3}{108 \cdot 10^6}\right) = 0.000329 \text{ m or } 0.329 \text{ mm}$$

The value adopted for the effective thickness of the mirror (T) needed to be the most extensive and, therefore, 5.042 mm was used. Finally, the mirror plate's nominal thickness

(T_m) was determined using Equations (17) and (18). For Equation (18), the value of C_c was 3 mm and the value of C_t was zero. Therefore, we have:

$$T_{m1} = 5.042 + 3 + 0 = 8.042 \text{ mm}$$

For Equation (19), the value of R_c was zero, as baffles were not being foreseen. Substituting the values, we have:

$$T_{m2} = 5.042 + 3 + 0 = 8.042 \text{ mm}$$

Thus, the value of the calculated mirror plate's nominal thickness (t) was 8.042 mm. Considering the commercial sheet thickness, which is higher and closer to the estimated value, the selected value is 8.5 mm and weighs 66.64 kg m^{-2} .

Caps Sizing

For the heat exchanger under analysis, the top and bottom caps were designed and manufactured following the specifications from the standard ASTM A 285 Gr C [45]. The minimum thickness of caps (T_{cap}) flanged and bolted was determined by Equation (23) [19,20]:

$$T_{cap} = d \sqrt{\frac{0.3 \cdot P}{S_{cap}}} \quad (23)$$

where d is the internal diameter of the cap (m), P is the design pressure (Pa), and S_{cap} = the allowable tension of the cap material (Pa). Considering that d totaled 0.2545 m, P totaled 248.42 kPa (Table 1), and S_{cap} totaled 108 MPa, and substituting these values, we have:

$$T_{cap} = 0.2545 \sqrt{\frac{0.3 \cdot 248.42 \cdot 10^3}{108 \cdot 10^6}} = 0.00668 \text{ m or } 6.68 \text{ mm}$$

The commercial wall thickness value adopted was 6.7 mm, weighing 52.59 kg/m. Eight machine screws and eight nuts with a nominal diameter of 1/2 inch, a hexagonal shape, an ASTM A-307 [46] specification, and being equally spaced, were used. The cap at the bottom served as a collector for the wood vinegar and wood tar, requiring a drop in the direction of the outlet pipe nozzle to facilitate the flow of fluids and avoid accumulation and, consequently, clogging.

Hydrostatic Pressure Test (PTH)

The results of the hydrostatic test pressure needed to reach at least 1.3 times the MAWP [27,28]. With the MAWP value at 0.283 MPa, the hydrostatic test pressure (PTH) needed to be $1.3 \times 0.283 \text{ MPa}$, namely 0.368 MPa.

2.4. Smoke Burner

The smoke burner was built in a cylindrical shape (combustion chamber and heat exchanger) so that the effects of thermal expansion and the intensity of heat that reaches the walls were symmetrical, contributing to the uniform distribution of the heat generated during combustion throughout the structure. A "V" shaped cover was installed at the top of the chimney to facilitate the flow of gases into the atmosphere. The main parameters for correctly sizing a smoke burner were the volume of the combustion chamber, the grate area, and the primary and secondary air openings, as detailed hereafter.

Smoke Burner Sizing

The smoke burner's primary function is to reduce the emission of pollutant gases, which occurs during the operation of the burner. Furthermore, the heat generated by burning wood in the burner helps direct gases out of the system, accelerating the ignition process [47]. According to Silva [48], the smoke burner should be composed of a combustion

chamber for combustion of gases, a grate, where the solid fuel is supported by inlet and outlet openings intended for loading the solid fuel and input of air, and an ashtray, where the combustion residues are deposited. This must have minimum dimensions but be sufficient for efficient combustion.

The proposed burner in this work was constructed with a double layer of solid ceramic bricks measuring 180 mm × 90 mm × 57 mm, laid with a mortar made from clay soil, washed sand, and water. It was proposed to adopt a square-shaped burner, with dimensions 1200 mm × 1180 mm × 5000 mm, with the internal part covered by a ceramic blanket adhered with the same mortar used in the construction to maintain interior heat and durability during the combustion. An opening of 250 mm × 250 mm was included for inserting firewood to feed the burner occasionally. The burner consisted of a supply system for gases from the kilns, a combustion chamber, an air intake system, and a chimney to cover the entire volume of gases generated in the three kilns, operating simultaneously. A cover with a specific triangular geometry was also designed to facilitate the exit of products generated by completely burning combustion gases in the smoke burner.

Average Specific Mass of Smoke Gases

One of the great technical challenges faced while burning carbonization gases is the wide variation in their composition, which can include more than 300 chemical components. Therefore, an approximate average value was calculated to determine the specific mass of the gases, considering the smoke burner would act under average temperature and pressure conditions by approaching the behavior of an ideal gas. Then, the average specific mass of the smoke was determined using the equation of state for perfect gases (Equation (24)):

$$\rho_{\text{sgases}} = \frac{P_{\text{atm}}}{R_{\text{sgases}} \cdot T_{\text{sgases}}} \quad (24)$$

where P_{sgases} is the average specific mass of smoke gases (kg m^{-3}), P_{atm} is the atmospheric pressure (kN m^{-2}), R_{sgases} is the universal constant of smoke gases ($\text{kNm kg}^{-1} \text{K}^{-1}$), and T_{sgases} is the average temperature of the smoke (K).

According to Silva et al. [13], the average composition of the non-condensable portion of the smoke gases is composed of nitrogen (N_2)—67.8%, oxygen (O_2)—15.69%, carbon dioxide (CO_2)—11.82%, and carbon monoxide (CO)—3.84%. For such a mixture, the values of the universal gas constant are close to that of air ($0.287 \text{ kJ kg}^{-1} \text{ K}^{-1}$), according to [31]. Therefore, the universal gas constant was used in the calculations, having air as a reference. For temperature, the gas entry temperature into the burner (T_{ent}) was considered equal to 115 °C (see Table 1), and the gas exit temperature from the burner (T_{exit}) was equal to 850 °C, according to Cardoso [49]. Furthermore, we calculated that P_{atm} equaled 101.325 atm. Therefore, we have:

$$\rho_{\text{sgases}} = \frac{101.325}{0.287 \cdot 735} = 0.480 \frac{\text{kg}}{\text{m}^3}$$

Mass Flow Rate of Smoke Gases

The mass flow rate of smoke gases (\dot{m}_{sgases}) was determined using Equation (25), according to Melo et al. [24]:

$$\dot{m}_{\text{sgases}} = \rho_{\text{sgases}} \cdot \dot{V}_{\text{sgases}} \quad (25)$$

where \dot{m}_{sgases} is the mass flow rate of smoke gases (kg h^{-1}) and \dot{V}_{sgases} is the volumetric flow of smoke gases ($\text{m}^3 \text{ h}^{-1}$).

Considering the average specific mass of air calculated in Equation (25) and the volumetric flow of $3718.68 \text{ m}^3 \text{ h}^{-1}$, according to average data presented by Cardoso [49], we have:

$$\dot{m}_{\text{sgases}} = 0.480 \frac{\text{kg}}{\text{m}^3} \cdot 3718.68 \frac{\text{m}^3}{\text{h}} = 1784.97 \frac{\text{kg}}{\text{h}}$$

Amount of Heat Required to Burn Smoke Gases

The amount of energy (heat) required to burn gases (\dot{Q}) is determined by Equation (26), according to Silva et al. [48]:

$$\dot{Q} = \dot{m}_{\text{sgases}} \cdot c_p \cdot \Delta T \quad (26)$$

where \dot{Q} is the amount of heat required to burn smoke gases (kJ h^{-1}), c_p is the average specific heat of smoke gases ($\text{kJ kg}^{-1} \text{ K}^{-1}$), and ΔT is the temperature variation (K).

As cited previously, the average composition of the non-condensable portion of the smoke gases contains nitrogen, oxygen, carbon dioxide, and carbon monoxide. For all those gases, their specific heat values are close to air ($1.005 \text{ kJ kg}^{-1} \text{ K}^{-1}$), according to Cengel [31]. Therefore, this value was used as a reference. After substituting it into Equation (26), the result is as follows:

$$\dot{Q} = 1784.97 \frac{\text{kg}}{\text{h}} \cdot 1.005 \frac{\text{kJ}}{\text{kgK}} \cdot 735 \text{ K}$$

$$\dot{Q} = 1,318,512.71 \frac{\text{kJ}}{\text{h}}$$

Rate of Fuel to Be Consumed by the Smoke Burner

After determining the amount of energy (heat) required to burn the smoke gases per unit of time, the fuel consumption (rate) is specified, to meet the demand for energy needed, according to Equation (27) [24]:

$$\dot{m}_c = \frac{\dot{Q}}{\eta \cdot \text{PCI}} \quad (27)$$

where \dot{m}_c is the fuel rate to be consumed by the smoke burner (kg h^{-1}), η is the thermal efficiency of the smoke burner, and LHV is the lower heating value of the fuel (kJ kg^{-1}).

To determine the thermal efficiency of the smoke burner, an estimate was made based on the work of Melo et al. [24] and Silva et al. [48], who estimated values between 45 and 55%. Therefore, the average value of 50% was used in the calculations. The calorific value of a fuel is the amount of energy, in the form of heat, released in the complete combustion of a unit of mass or volume of a given fuel and does not depend on the conditions under which it is burned, since combustion is considered complete of it; it is generally divided into lower (LHV) and upper (UHV) calorific value. The upper calorific value can be estimated from the chemical composition of the fuel or calculated using an experimental method, while the lower calorific value is calculated from empirical equations [50]. The LHV can be calculated using the following equation, known as the Dulong formula [51]:

$$\text{LHV} = \text{HHV} - 2450(9 \cdot P_{\text{H}_2}) \quad (28)$$

where LHV is the lower heating value of the fuel (kJ kg^{-1}), HHV is the higher heating value of the fuel (kJ/kg), and P_{H_2} is the fraction of hydrogen in the fuel ($\text{kg of hydrogen per kg of fuel}$), which is considered to have a value of 0.038, according to Silva et al. [48].

The fuel used to power the smoke burner comes from mesquite residue, a tree typical of Northeastern Brazil and, therefore, easily accessible. Furthermore, according to Cavalcanti et al. [52], the HHV of mesquite is $18,940 \text{ kJ kg}^{-1}$ higher than the calorific value

of several solid fuels of vegetable origin, highlighting the possibility of its use as an energy product. Therefore, substituting the values into Equation (28), we have:

$$\text{LHV} = 18,940 \frac{\text{kJ}}{\text{kg}} - 2450(9 \cdot 0.038) = 18,102.1 \frac{\text{kJ}}{\text{kg}}$$

Then, the fuel rate to be consumed by the smoke burner (\dot{m}_c) is determined by substituting the values into Equation (27), thus, we have:

$$\dot{m}_c = \frac{1,318,512.71 \frac{\text{kJ}}{\text{h}}}{0.5 \cdot 18,102.1 \frac{\text{kJ}}{\text{kg}}} = 145.68 \frac{\text{kg}}{\text{h}}$$

Combustion Chamber Volume

To calculate the volume of the combustion chamber (V_{cc}), Equation (29) was employed, according to Melo et al. [24]:

$$V_{cc} = \frac{\dot{m}_c \cdot \text{LHV}}{K} \quad (29)$$

where V_{cc} is the combustion chamber volume (m^3), \dot{m}_c is the fuel rate (kg h^{-1}), and K is the energy release rate ($\text{kJ m}^{-1} \text{h}^{-1}$). The average value adopted [51] was $734,400 \text{ kJ m}^{-1} \text{h}^{-1}$. Substituting the values, we have:

$$V_{cc} = \frac{145.68 \frac{\text{kg}}{\text{h}} \cdot 18,102.1 \frac{\text{kJ}}{\text{kg}}}{734,400 \frac{\text{kJ}}{\text{m}^3\text{h}}} = 3.59 \text{ m}^3$$

Grate Surface Area

The grate surface area was determined as a function of the combustion rate (N_c) for design purposes, which, in this case, gave the formula (Equation (30)):

$$S_g = \frac{\dot{m}_c}{\left(\frac{N_c}{3600}\right)} \quad (30)$$

where S_g is the grate surface area (m^2) and N_c is the combustion rate ($\text{kg m}^{-2} \text{h}^{-1}$), the value of which was set at $150 \text{ kg m}^{-2} \text{h}^{-1}$ (based on Melo et al. [24]). Substituting the values, the result is:

$$S_g = \frac{145.68 \frac{\text{kg}}{\text{h}}}{150 \frac{\text{kg}}{\text{m}^2\text{h}}} = 0.97 \text{ m}^2$$

Fans

Two axial fans with a diameter of 200 mm and a power of 0.5 CV and 220 V, were installed, opposed, and inclined at 30° to the vertical, with the primary function of accelerating the transport of the product from the burning of gases (CO_2 and H_2O) out of the smoke burner, optimizing the process.

3. Results

The final structure of the carbonization kilns is displayed in Figures 3 and 4.

In Figure 5, the collection of tubes (Figure 5A) and the final configuration of the condensing system (Figure 5B) are shown.

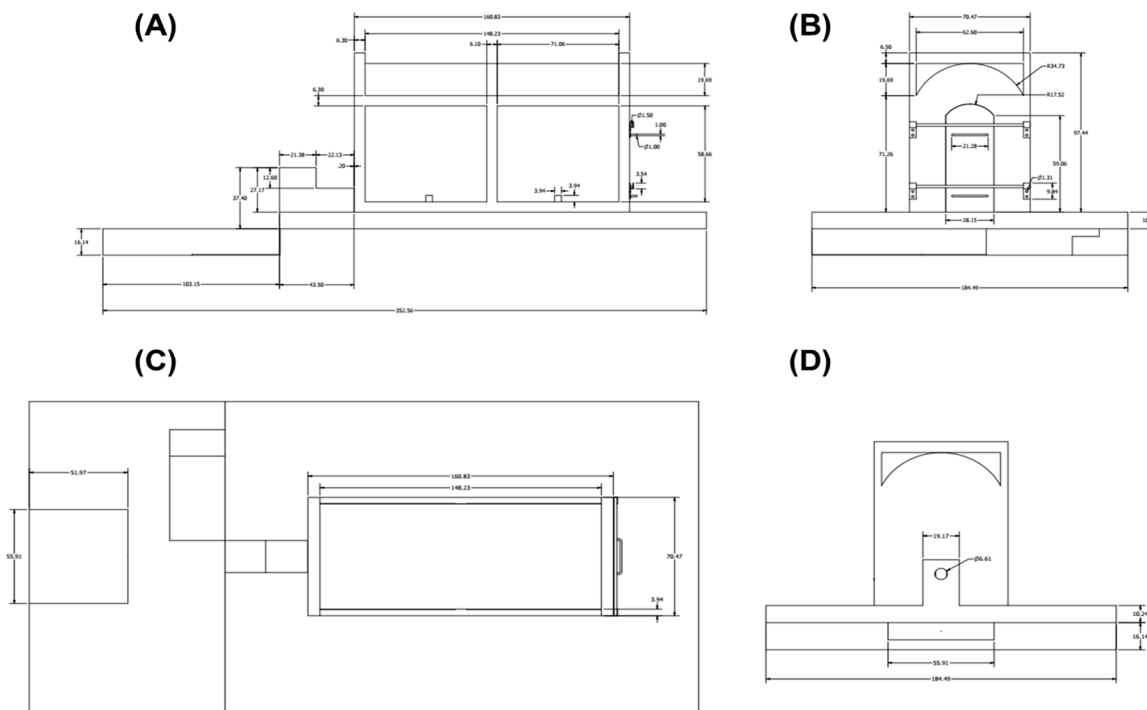


Figure 3. Views of the mini-kilm (dimensions in millimeters). (A) Side; (B) front; (C) top; and (D) rear view.

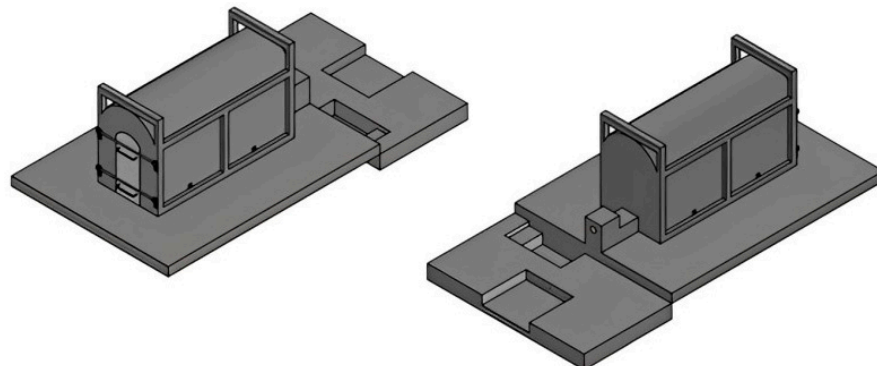


Figure 4. Front and rear three-dimensional drawings of the mini-kilm.

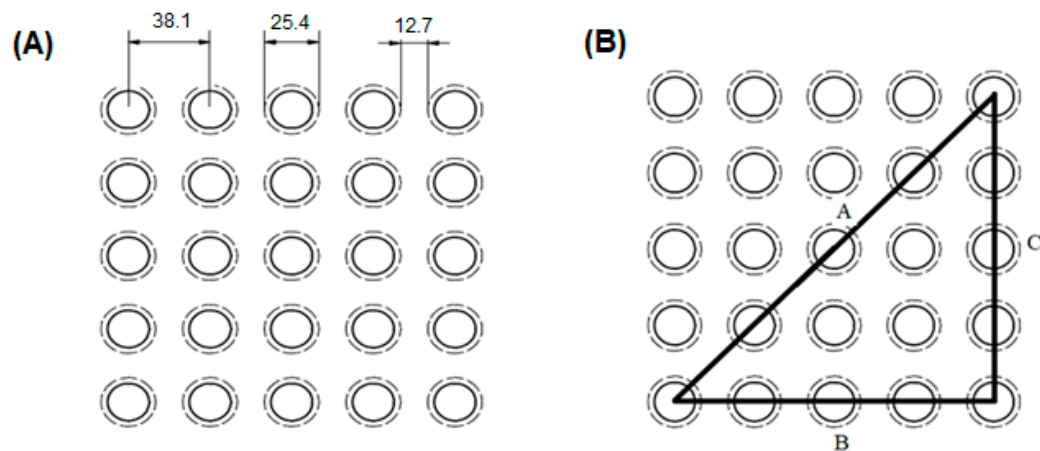


Figure 5. Arrangement of the set tubes of the condensing system (dimensions in mm) (A). Representation of the right-angled triangle formed by dividing the square (B).

The final arrangement of the condensing system is presented in different views and perspectives in Figures 6 and 7.

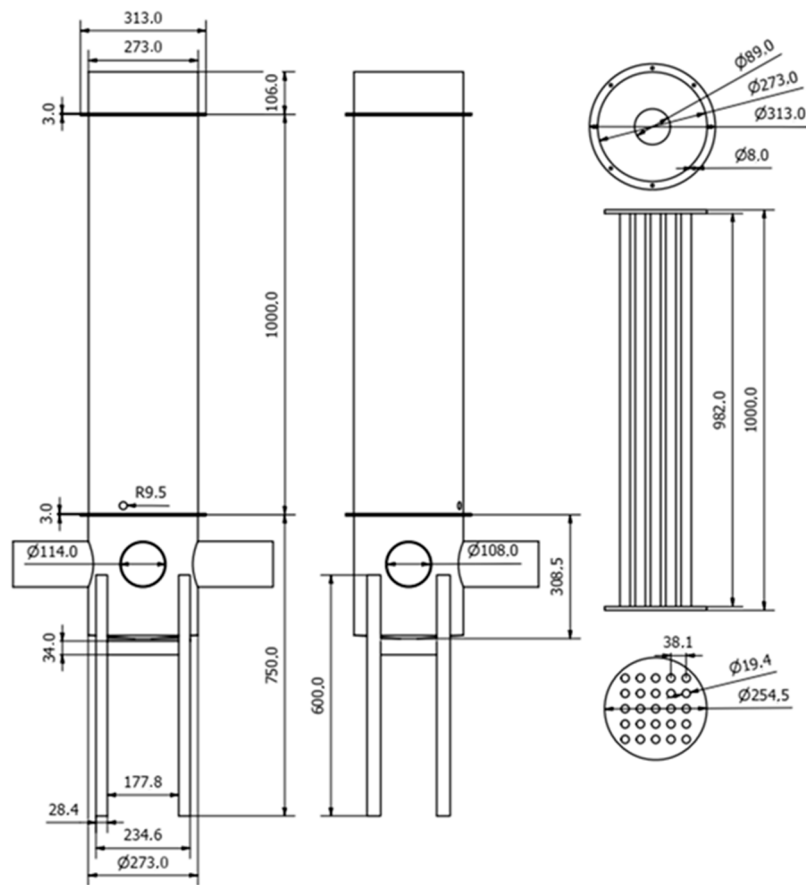


Figure 6. Condensing system in isometric perspective and orthographic views of the tube set (dimensions in mm).

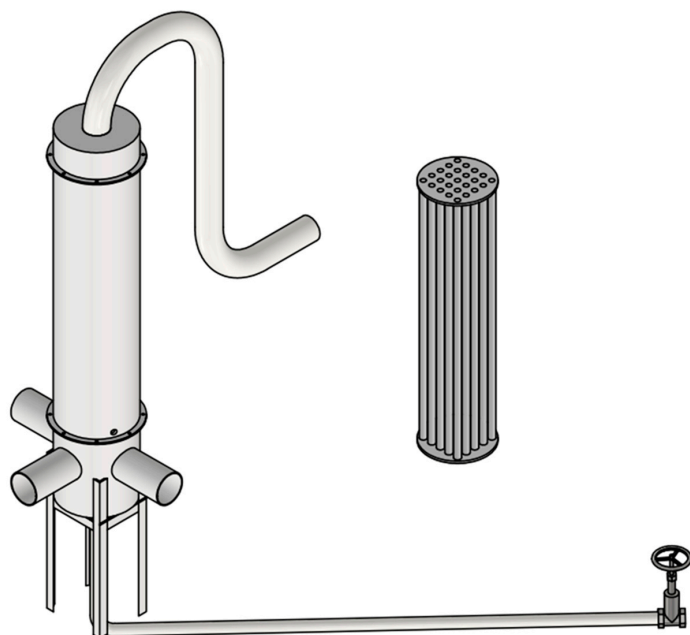


Figure 7. Three-dimensional view of the condensing system and the tube set.

The final drawings of the smoke burner in isometric and other perspectives can be seen in Figures 8 and 9.

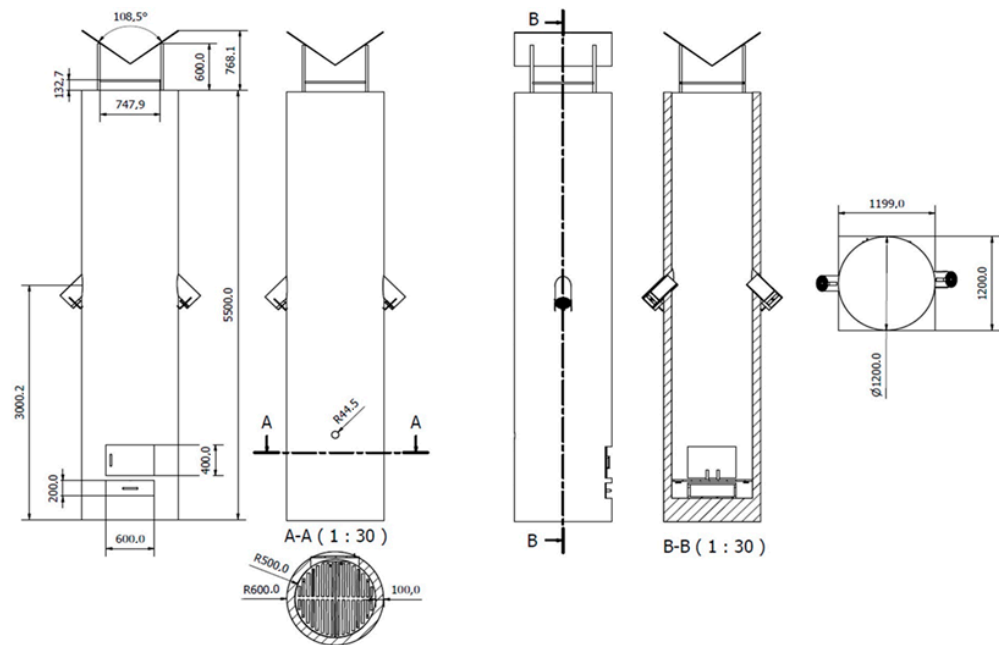


Figure 8. Smoke burner in isometric perspective and orthographic views (dimensions in mm).

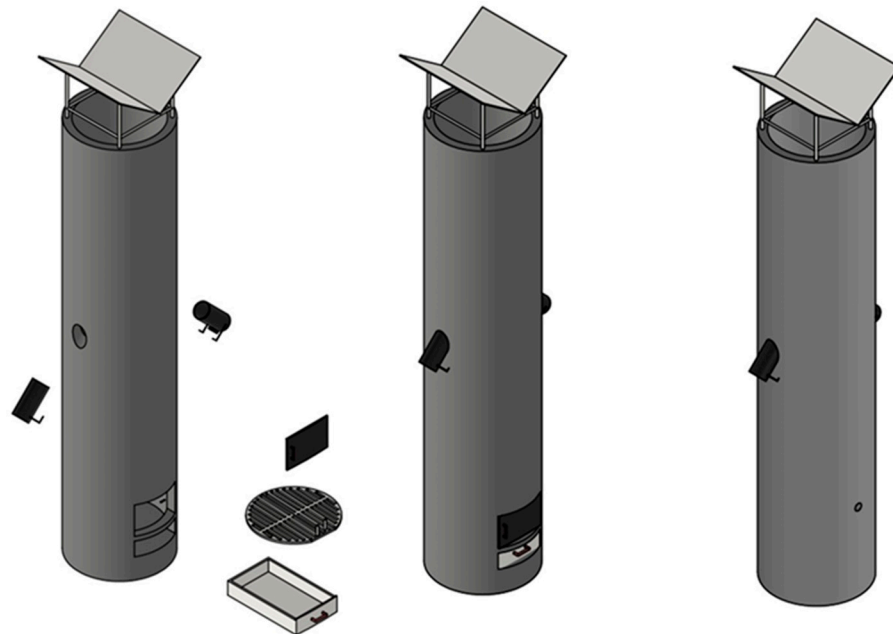


Figure 9. Three-dimensional views of the smoke burner from different perspectives.

As commented previously, the integrated set, intended to produce charcoal and wood vinegar on a small scale, consisted of a set of three kilns, a condensing system, and a smoke burner (Figures 10 and 11). In this way, the same condenser/burner set is used by the three kilns. The vertical smoke burner was designed to be coupled to the condensing system.

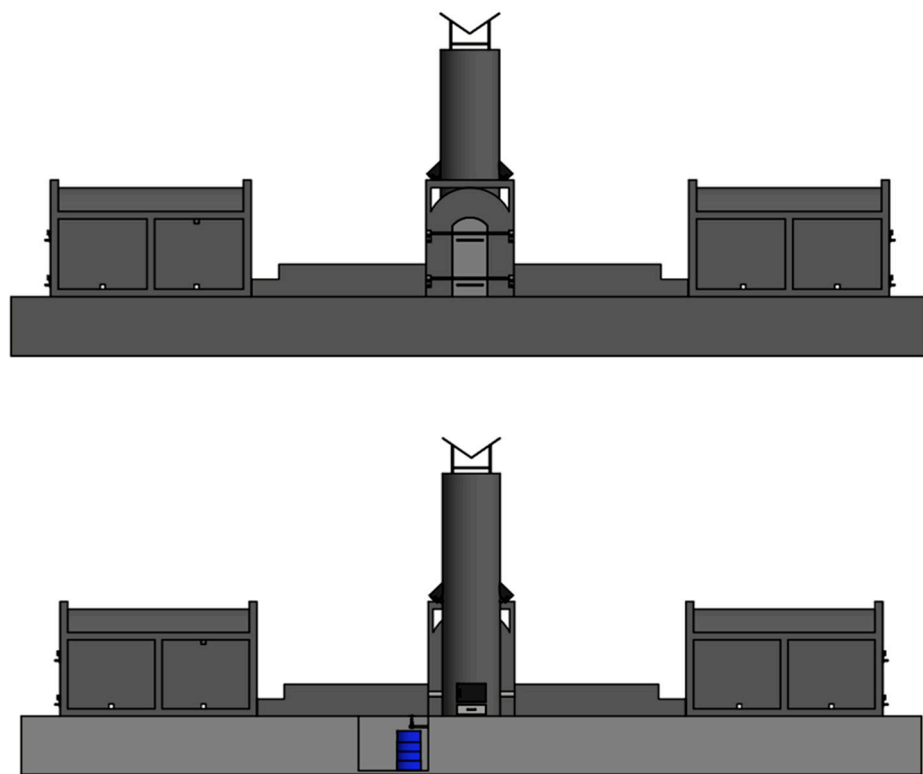


Figure 10. Front and rear views of the kilns, condensing device, and smoke burner from different views.

In northeastern Brazil, the wood carbonization process is still carried out in rudimentary kilns and even in open pits in the ground; these processes have low mass and energy yields and are very polluting. In these primitive production processes, the gravimetric charcoal yield rarely exceeds 20%. In rectangular masonry kilns, this yield can be higher than 30%, maximizing the use of firewood and generating extra income for the charcoal-maker. Therefore, projects that feature carbonization kilns intended for use on small and medium-sized rural properties can help to produce charcoal efficiently.

Furthermore, these projects can enable the recovery of co-products such as wood vinegar (WV), which, in traditional processes, are released directly into the atmosphere. With this, small producers can produce charcoal and WV on their property, increasing their monthly income, through a carbonization technique that is less harmful to the producer and the environment. With this study, it was possible to present to a small producer in the semi-arid region a proposal for a set of three low-cost and environmentally friendly mini-kilns coupled to a condensing system for WV recovery. Additionally, the integration of the system with a smoke burner was proposed, reducing the emission of polluting gases into the atmosphere.

For any changes in the parameters used in this work, such as the dimensions of the equipment, fluids, and materials used, the chemical, mechanical, and thermal properties, and the conditions of use of the analyzed equipment, all calculations must be redone.

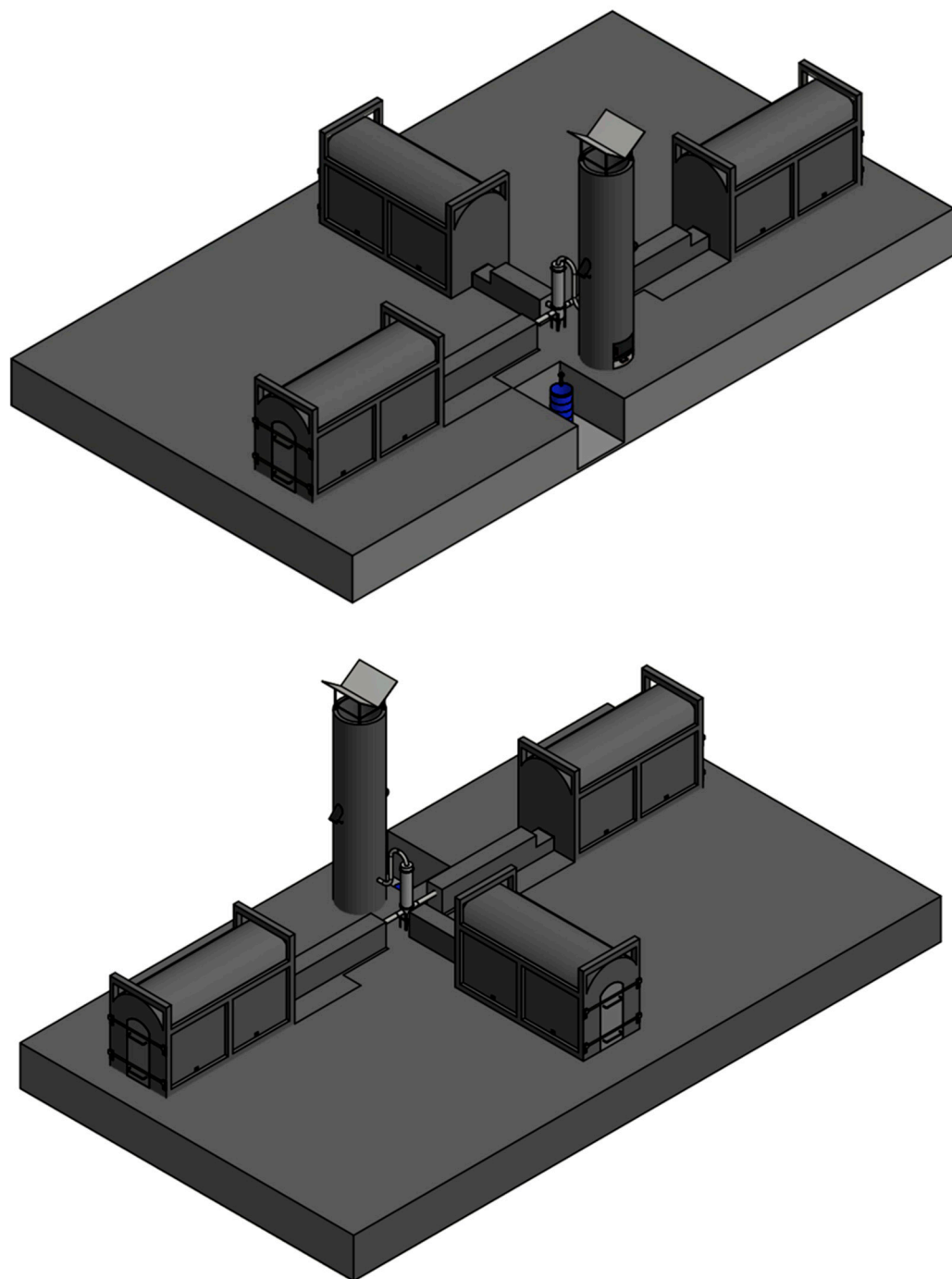


Figure 11. Three-dimensional views of the carbonization set (kilns, condensing device, and smoke burner) from different perspectives.

4. Discussion

In the design process, some process variables related to gases from combustion were estimated (i.e., the mass flow rate and the global heat transfer coefficient). For the variables of specific heat (c_p) and enthalpy of vaporization (h_{fg}), the acceptable values were estimated, due to the high heterogeneity in the composition of the raw material.

In the thermal project, it was initially assumed that the fluids involved have a permanent flow rate, with changes in kinetic and potential energy being insignificant, that heat conduction in the axial direction is negligible, and that the external surface of the heat exchanger is perfectly isolated, with no exchange of heat with the environment occurring. To calculate the heat exchange area, the logarithmic mean temperature difference method

(LMDT) was used, as it was possible to estimate the inlet and outlet temperatures of the fluids. From this, it was calculated that 25 tubes would be needed for the bundle of tubes. The parameters were calculated using the specification ASTM A179 [41], resulting in a square arrangement, a length of 0.8 m, a center-to-center spacing of 38.1 mm, and a total heat exchange area of 1.56675 m^2 ; it was also calculated that the nominal diameter of the shell would be 10 in (from = 273 mm) with an internal diameter of 254.5 mm and a wall thickness of 9.27 mm, corresponding to "Series 40" or "Std", and with an approximate weight of 60.23 kg/m.

In the mechanical design, the condenser (heat exchanger) was initially classified as class C according to ASME [28] and TEMA [27]; the shell would have a tubular shape, as this is easier to manufacture and transport, being manufactured from ASTM A53 Gr A [44], with its dimensions, previously calculated in the thermal project, confirmed, considering a corrosion over-thickness of 3 mm. The tube bundle had its dimensions calculated in the thermal design, with a wall thickness of 2.77 mm. The PMTA was 0.283 MPa, a value determined by considering that the most critical part of the vessel internally is the external side of the tubular bundle. The mirrors would be manufactured from sheet metal with ASTM A285 Gr C [45] specification, a commercial wall thickness of 8.5 mm, and a 66.64 kg/m weight. They must be manufactured fixed to the hull without considering the effects of expansion as the heat exchanger. They will work with a low-temperature difference, with the ideal temperature being between 115 °C and 150 °C, simplifying construction and assembly. A drop must be provided on the spool lid at the bottom, in the direction of the pipe nozzle, to collect the pyroligneous extract and vegetable tar from the outlet, in order to facilitate the flow of fluids and thus avoid accumulation. The hydrostatic test pressure (PTH) was calculated to be 0.368 MPa.

The calculated wall thickness values corresponded to minimum operating values; therefore, if using the materials with the calculated thickness values is impossible, they must be replaced by another material with equal properties and a commercial wall thickness equal to or immediately higher the calculated value.

When sizing the heat exchanger, fluid changes, pressure variations, temperature variations, and welded joints were not considered, nor were calculations made for supports, sealing joints, and flange screws.

When sizing the smoke burner, the reference parameters (energy release rate, combustion rate, yield, and volumetric flow of gases) were based on works that used furnaces intended for other purposes, such as coffee and wood drying, to arrive at the proposed model. The fuel used to power the smoke burner comes from mesquite residue, a tree typical of the northeast region and, therefore, easily accessible. The fans used were proposed by the models currently sold. Furthermore, an ashtray was provided to remove residue from the burner, facilitating cleaning. At the top of the smoke burner is a "V" shaped screen to facilitate the exit of gases from the burning.

5. Conclusions

The proposed kiln system was designed to be manufactured with ceramic bricks to reduce heat losses during carbonization and maximize the charcoal yield while allowing fast cooling after the carbonization is concluded. Each oven has five holes, four at the base of opposing side walls to control oxygen entry and one at the top of one for ignition. The number of kilns meets the parameters related to optimization, considering that the average pyrolysis time is approximately eight days, where, for each oven, 2 h are used to load firewood, 72 h for carbonization, 120 h for cooling and 2 h for unloading the coal, totaling 196 h. With this distribution, charcoal production is maintained uninterrupted, and the recovery of wood vinegar is possible, since all kilns are connected to the condenser individually. Therefore, there will always be a kiln conducting carbonization, another performing the cooling process, and another unloading charcoal and loading firewood. This way, as soon as one carbonization run ends, another occurs, and the process continues.

The condensation system for recovering the wood vinegar was designed in accordance with current national and international standards for heat exchangers and pressure vessels. In addition, analyses and applications adopted by renowned authors in the area were considered to constitute a logical sequence for the calculations, adopting values in line with those used in the current production system from a functional and commercial point of view. That said, the system is feasible and can be adopted by small producers, guaranteeing operational safety. In turn, the smoke burner plays a fundamental role in the system as it completely burns carbonization gases, reducing the pollution released into the atmosphere. The sizing considered the average type of wood feeding the kilns. Also, the wood calorific value, the average composition of carbonization gases, the mass flow rate of gases, the volumetric flow rate of gases, and the average specific heat of gases were fundamental to the sizing. The structure was designed to be manufactured using the same type of refractory bricks used in the furnace system, aiming for the same operational gains. Furthermore, the geometry of the smoke burner was designed to facilitate the supply of wood, removal of ash, and flow of gases.

Given this, the proposed mini-kiln system adds technological value to the system to guarantee the operational safety of the process, in addition to opening ways for the small-scale production of wood vinegar and charcoal, with a higher added value as research advances. Therefore, small farmers can produce charcoal and wood vinegar on their property in an optimized and low-cost way, increasing their monthly income and promoting the circular economy through a carbonization technique that is less harmful to the producer and the environment. In contrast to the current scenario, in which primitive carbonization technologies are still employed, bringing about low charcoal yields and significant pollution release, using a mini-kiln that allows charcoal production and wood vinegar recovery, combined with pollutant smoke burning, is an interesting eco-friendly solution.

Author Contributions: Conceptualization, F.B.d.A., R.R.d.M. and A.S.P.; methodology, F.B.d.A. and A.S.P.; software, E.A.d.O.P.; validation, M.V.S. and F.R.; formal analysis, E.A.d.O.P., M.V.S., F.R. and R.R.d.M.; investigation, F.B.d.A.; resources, R.R.d.M. and A.S.P.; data curation, R.R.d.M., F.R. and M.V.S.; writing—original draft preparation, F.B.d.A., R.R.d.M. and A.S.P.; writing—review and editing, E.A.d.O.P., M.V.S. and F.R.; visualization, R.R.d.M. and A.S.P.; supervision, R.R.d.M., F.R. and M.V.S.; project administration, R.R.d.M.; funding acquisition, R.R.d.M. and A.S.P. All authors have read and agreed to the published version of the manuscript.

Funding: The study was financed by the Brazilian Ministry of Regional Development (MDR) through the Sabiá platform and Guimarães Duque Foundation (FGD). Additionally, financial support was provided in part by the Brazilian National Council for Scientific and Technological Development (CNPq).

Data Availability Statement: Raw data were generated at the UFERSA and UFRN (Brazilian Universities). Derived data supporting the findings of this study are available from the corresponding author upon request.

Acknowledgments: We express our thanks to the Office to Coordinate Improvement of Higher Education Personnel (CAPES) for granting graduate scholarships (Financial Code 001).

Conflicts of Interest: All authors agree with this submission and declare there are no potential competing interests related to content either financial or non-financial interests to disclose.

References

1. Rodrigues, T. Model for the Conceptual Projects Development of Carbonization Kiln. Ph.D. Thesis, Universidade Tecnológica Federal do Paraná, Ponta Grossa, Brazil, 2019.
2. Zola, F.C.; Colmenero, J.C.; Aragão, F.V.; Rodrigues, T.; Braghini, A., Jr. Multicriteria model for selecting a charcoal kiln. *Energy* **2020**, *190*, e116377. [[CrossRef](#)]
3. IBÁ—Indústria Brasileira de Árvores. Relatório Anual Estatístico de 2021: Ano Base 2020. 2022. Available online: <https://www.iba.org/publicacoes/relatorios> (accessed on 20 January 2023).
4. Pereira, E.G.; Fauller, H.; Magalhães, M.; Guirardi, B.; Martins, M.A. Potential use of wood pyrolysis coproducts: A review. *Environ. Prog. Sustain. Energy* **2022**, *41*, e13705. [[CrossRef](#)]

5. Paradela, F.M.R. Study of the Pyrolysis of Mixtures of Plastic Waste, Tires and Biomass. Ph.D. Thesis, Universidade Nova de Lisboa, Lisboa, Portugal, 2012.
6. Farias, S.P.; Almeida, A.V.D.L.; Nascimento, E.S.; SolettI, J.I.; Balliano, T.L.; Moura Filho, G.; Muniz, M.F.S. In vitro and in vivo control of yam dry rot nematodes using pyroligneous extracts from palm trees. *Rev. Ceres* **2020**, *67*, 482–490. [[CrossRef](#)]
7. Biscaia, R.V.B. Methodology for the Development of a Transportable Carbonization Kiln Project. Ph.D. Thesis, Universidade de São Paulo, São Paulo, Brazil, 2021.
8. Fedeli, R.; Vannini, A.; Grattacaso, M.; Loppi, S. Wood distillate (pyroligneous acid) boosts nutritional traits of potato tubers. *Ann. Appl. Biol.* **2023**, *183*, 135–140. [[CrossRef](#)]
9. Grewal, A.; Abbey, L.; Gunupuru, L.R. Production, prospects and potential application of pyroligneous acid in agriculture. *J. Anal. Appl. Pyrolysis* **2018**, *135*, 152–159. [[CrossRef](#)]
10. Rodrigues, T.; Braghini Junior, A. Charcoal: A discussion on carbonization kilns. *J. Anal. Appl. Pyrolysis* **2019**, *143*, 104670. [[CrossRef](#)]
11. Gama, G.S.P.; Pimenta, A.S.; Feijó, F.M.C.; Santos, C.S.; Fernandes, B.C.C.; Oliveira, M.F.; Souza, E.C.; Monteiro, T.V.C.; Fasciotti, M.; Azevedo, T.K.B.; et al. Antimicrobial activity and chemical profile of wood vinegar from eucalyptus (*Eucalyptus urophylla × Eucalyptus grandis* – clone I144) and bamboo (*Bambusa vulgaris*). *World J. Microbiol. Biotechnol.* **2023**, *39*, 186. [[CrossRef](#)]
12. Morales, M.M.; Sartori, W.W.; Silva, B.R.; Spera, S.T.; Mendes, A.B.D.; Albuquerque, E.P.A. Wood vinegar: Chemical characteristics, phytotoxic effects, and impacts on greenhouse gas emissions. *Nativa* **2022**, *10*, 400–409. [[CrossRef](#)]
13. Silva, C.J.; Arruda, T.P.M.; Diodato, M.A. Pyroligneous extract of *Enterolobium contortisiliquum* (Vell.) Morong, against termite attack on lumber of *Aspidospoma polyneuron* Müll. *Arg. Nativa* **2022**, *10*, 387–390. [[CrossRef](#)]
14. Fedeli, R.; Fiaschi, T.; Angiolini, C.; Maccherini, S.; Loppi, S.; Fanfarillo, E. Dose-Dependent and Species-Specific Effects of Wood Distillate Addition on the Germination Performance of Threatened Arable Plants. *Plants* **2023**, *12*, e3028. [[CrossRef](#)]
15. Tiilikka, K.; Fagerås, L.; Tiilikka, J. History and Use of Wood Pyrolysis Liquids as Biocide and Plant Protection Product. *Open Agric. J.* **2010**, *4*, 111–118. [[CrossRef](#)]
16. Soares, W.N.C.; Lira, G.P.O.; Santos, C.S.; Dias, G.N.; Pimenta, A.S.; Pereira, A.F.; Benício, L.D.M.; Rodrigues, G.S.O.; Amora, S.S.A.; Alves, N.D.; et al. Pyroligneous acid from *Mimosa tenuiflora* and *Eucalyptus urograndis* as an antimicrobial in dairy goats. *J. Appl. Microbiol.* **2021**, *131*, 604–614. [[CrossRef](#)] [[PubMed](#)]
17. Feijo, F.M.C.; Fernandes, F.C.; Alves, N.D.; Pimenta, A.S.; Santos, C.S.; Rodrigues, G.S.O.; Pereira, A.F.; Benicio, L.D.M.; Moura, Y.B.F. Efficiency of Pyroligneous Extract from Jurema Preta (*Mimosa tenuiflora* [Willd.] Poiret) as an Antiseptic in Cats (*Felis catus*) Subjected to Ovariosalpingohysterectomy. *Animals* **2022**, *12*, 2325. [[CrossRef](#)] [[PubMed](#)]
18. Duan, D.; Chen, D.; Huang, L.; Zhang, Y.; Zhang, Y.; Wang, Q.; Xiao, G.; Zhang, W.; Hanwu, L.; Ruan, R. Activated carbon from lignocellulosic biomass as catalyst: A review of the applications in fast pyrolysis process. *J. Anal. Appl. Pyrolysis* **2021**, *158*, 105246. [[CrossRef](#)]
19. Gao, W.; Zhang, M.; Wu, H. Bed clumping during fast pyrolysis of bio-oil-derived fuels in a fluidized bed reactor. *Combustível* **2022**, *328*, 125359.
20. Sui, H.; Tian, C.; Chen, J.; Fullmer, S.; Zhang, Z. Characterization and separation of wood tar by full temperature range fractional distillation. *Sep. Purif. Technol.* **2022**, *302*, 122098. [[CrossRef](#)]
21. Silveira, C.S.; Oliveira, L. Analysis of the Carbon Market in Brazil: History and Development. *Novos Cad. NAEA* **2021**, *24*, 11–31.
22. Cardoso, M.T.; Carneiro, A.C.O.; Jacovine, L.A.G.; Vital, B.R.; Barcelos, D.C. Construction of a carbonization gas burning system to reduce pollutant emissions. *Cerne* **2010**, *16*, 115–124.
23. Gerdes, C.; Simon, C.M.; Ollesch, T.; Meier, D.; Kaminsky, W. Design, construction, and operation of a fast pyrolysis plant for biomass. *Eng. Life Sci.* **2002**, *2*, 167–174. [[CrossRef](#)]
24. Melo, F.A.O.; Silva, J.N.; Silva, J.S.; Sampaio, C.P.; Silva, D.F. Development and construction of a biomass furnace with direct and indirect air heating system. *Acta Sci. Technol.* **2010**, *32*, 129–136.
25. Oliveira, A.C. Kiln-furnace system for charcoal production. Ph.D. Thesis, Federal University of Viçosa, Viçosa, Brazil, 2012.
26. NBR 15270-1; Componentes Cerâmicos—Blocos e Tijolos para Alvenaria. Associação Brasileira de Normas Técnicas: Rio de Janeiro, Brazil, 2017; 71p.
27. TEMA. *Standards of Tubular Exchangers Manufactures Association*, 9th ed.; TEMA: New York, NY, USA, 2007.
28. ASME. *Boiler and Pressure Vessels Code*; American Society of Mechanical Engineers: New York, NY, USA, 2010; Section VIII, Division 1.
29. NR-13; Norma Regulamentadora 13—Caldeiras, Vasos de Pressão, Tubulações e Tanques Metálicos de Armazenamento. Portaria No. 1846, de 1 de julho de 2022; Ministério do Trabalho e Previdência: Brasília, Brazil, 2022.
30. Telles, P.C.S. *Vasos de Pressão*, 2nd ed.; LTC: Rio de Janeiro, Brazil, 2012; p. 298.
31. Cengel, Y.A.; Cimbala, J.M. *Mecânica dos Fluidos*, 3rd ed.; Amgh Editora: Manhattan, NY, USA, 2015; p. 1016.
32. Instituto Brasileiro do Meio Ambiente e dos Recursos Naturais Renováveis. *Manual de Construção e Operação do Forno Rabo Quente*; IBAMA: Brasilia, Brazil, 1999.
33. Lana, A.Q. Masonry Kiln to Increase Productivity through the External Cooling of Charcoal. Ph.D. Thesis, Universidade de São Paulo, São Paulo, Brazil, 2018.
34. Silva, P.A.; Salazar, C.I.S. Development of a programmable mathematical model for sizing a shell and tube heat exchanger. Ph.D. Thesis, Universidade Mackenzie, São Paulo, Brazil, 2020.

35. Campos, A.D. *Técnicas para Produção de Extrato Pirolenhoso para Uso Agrícola*; Ministério da Agricultura: Brasilia, Brazil, 2007; p. 8.
36. Zadeh, Z.; Abdulkhani, A.; Aboelazayem, O.; Saha, B. Recent Insights into Lignocellulosic Biomass Pyrolysis: A Critical Review on Pretreatment, Characterization, and Products Upgrading. *Process* **2020**, *8*, 799. [[CrossRef](#)]
37. Pires, A.; Arauzo, J.; Fonts, I.; Domine, M.E.; Arroyo, A.F.; Perez, M.E.G.; Montoya, J.; Chejne, F.; Pfromm, P.; Perez, M.G. Challenges and Opportunities for Bio-oil Refining: A Review. *Energy Fuels* **2019**, *33*, 4683–4720. [[CrossRef](#)]
38. Pereira, E.G.; Martins, M.A.; Paceka, R.; Carneiro, A.C.O. Pyrolysis gases burners: Sustainability for integrated production of charcoal, heat and electricity. *Renew. Sustain. Energy Rev.* **2017**, *75*, 592–600. [[CrossRef](#)]
39. Leme, M.M.V.; Venturini, O.J.V.; Lora, E.E.S.; Rocha, M.H.; Luz, F.C.; Almeida, W.; Moura, D.C.; Moura, L.F. Electricity generation from pyrolysis gas produced in charcoal manufacture: Technical and economic analysis. *J. Clean. Prod.* **2018**, *194*, 219–242. [[CrossRef](#)]
40. Schneider, M. *Tabela de Seleção de Bombas e Motobombas*; Franklin Eletric Indústria de motobombas S.A.: Rio de Janeiro, Brazil, 2019; Available online: https://schneidermotobombas.blob.core.windows.net/media/264019/schneider_tabela_selecao_012019_rev08.pdf (accessed on 17 November 2022).
41. ASTM, A179M-19; Standard Specification for Seamless Cold-Drawn Low-Carbon Steel Heat-Exchanger and Condenser Tubes. ASTM International: West Conshohocken, PA, USA, 2019.
42. ASME B31.3; Process Piping. American Society of Mechanical Engineers: New York, NY, USA, 2020.
43. Telles, P.C.S.; Barros, D.G.P. *Tubulações Industriais: Tabelas e Gráficos*, 6th ed.; LTC: Rio de Janeiro, Brazil, 2008; p. 190.
44. ASTM, A53M-22; Standard Specification for Pipe, Steel, Black and Hot-Dipped, Zinc-Coated, Welded and Seamless. ASTM International: West Conshohocken, PA, USA, 2022.
45. ASTM, A285M-17; Standard Specification for Pressure Vessel Plates, Carbon Steel, Low- and Intermediate-Tensile Strength. ASTM International: West Conshohocken, PA, USA, 2017.
46. ASTM, A307-21; Standard Specification for Carbon Steel Bolts, Studs, and Threaded Rod 60,000 psi Tensile Strength. ASTM International: West Conshohocken, PA, USA, 2021.
47. Schettini, B.L.S.; Jacobine, L.A.G.; Torres, C.M.M.E.; Carneiro, A.C.O.; Villanova, P.H.; Rocha, S.J.S.S.; Rufino, M.P.M.X.; Silva, L.B.; Castro, R.V.P. Furnace-kiln system: How does the use of new technologies in charcoal production affect the carbon balance? *Ind. Crops Prod.* **2022**, *187*, 115330. [[CrossRef](#)]
48. Silva, I.D.; Silva, J.N. Design, construction and test of a charcoal furnace for drying of coffee without pulp/hull. *Rev. Bras. Eng. Agríc. Ambient.* **1998**, *2*, 301–307. [[CrossRef](#)]
49. Cardoso, M.T. Performance of a System Oven-Furnace for Combustion of Gases from Wood Carbonization. Master’s Dissertation, Universidade Federal de Viçosa, Viçosa, Brazil, 2010.
50. Andrade, E.B.; Sasseron, J.L.; Oliveira Filho, D. *Princípios Sobre Combustíveis, Combustão e Fornalhas*; UFV: Viçosa, Brazil, 1985; p. 8.
51. Silva, I.D. Project, construction and test of a charcoal furnace for coffee drying. Marster’s Dissertation, Universidade Federal de Viçosa, Viçosa, Brazil, 1998.
52. Cavalcanti, I.L.R.; Moura, I.A.A.; Cruz, A.D.; Silva, M.C.D.; Lopes, R.M.B.P. Chemical characterization of algaroba biomass waste for energy studies. *Braz. J. Dev.* **2020**, *6*, 872–881. [[CrossRef](#)]

Disclaimer/Publisher’s Note: The statements, opinions and data contained in all publications are solely those of the individual author(s) and contributor(s) and not of MDPI and/or the editor(s). MDPI and/or the editor(s) disclaim responsibility for any injury to people or property resulting from any ideas, methods, instructions or products referred to in the content.